HOKKAIDO UNIVERSITY

Title	The Impact of Tortuosity on Chloride Ion Diffusion in Slag-Blended Cementitious Materials
Author(s)	Hatanaka, Akira; Elakneswaran, Yogarajah; Kurumisawa, Kiyofumi et al.
Citation	Journal of advanced concrete technology, 15(8), 426-439 https://doi.org/10.3151/jact.15.426
Issue Date	2017-08
Doc URL	https://hdl.handle.net/2115/68220
Type	journal article
File Information	15_426.pdf



Hokkaido University Collection of Scholarly and Academic Papers : HUSCAP

Journal of Advanced Concrete Technology
Materials, Structures and Environment

The Impact of Tortuosity on Chloride Ion Diffusion in Slag-Blended Cementitious Materials

Akira Hatanaka, Yogarajah Elakneswaran, Kiyofumi Kurumisawa, Toyoharu Nawa

Journal of Advanced Concrete Technology, volume 15 (2017), pp. 426-439

Related Papers Click to Download full PDF!

Multi-scale Modeling of Concrete Performance- Integrated Material and Structural Mechanics
Koichi Maekawa, Tetsuya Ishida, Toshiharu Kishi
Journal of Advanced Concrete Technology, volume 1 (2003), pp. 91-126

Effect of the key mixture parameters on tortuosity and permeability of concrete
Shamsad Ahmed, Abul Kalam Azad, Kevin F. Loughlin
Journal of Advanced Concrete Technology, volume 10 (2012), pp. 86-94

Enhanced model and simulation of hydration process of blast furnace slag in blended cement
Yao Luan, Tetsuya Ishida, Toyoharu Nawa, Takahiro Sagawa
Journal of Advanced Concrete Technology, volume 10 (2012), pp. 1-13

Click to Submit your Papers
Japan Concrete Institute http://www.j-act.org

Scientific paper

The Impact of Tortuosity on Chloride Ion Diffusion in Slag-Blended Cementitious Materials

Akira Hatanaka[1], Yogarajah Elakneswaran[2*], Kiyofumi Kurumisawa[3] and Toyoharu Nawa[4]

Received 26 December 2016, accepted 19 August 2017 doi:10.3151/jact.15.426

Abstract

The purpose of this study is to determine the tortuosity of cementitious materials containing blast furnace slag (BFS). Furthermore, the influence of tortuosity on multi-species transport into these materials is studied. The porosity and diffusivity of calcium silicate hydrate (C-S-H) were predicted using a three-dimensional spatial distribution model, which were then fitted to Archie's law to determine tortuosity. The tortuosity increased with the slag replacement ratio, suggesting that the diffusion path for ions becomes complicated and lengthy due to slag addition. Thermoporometry was used to determine the pore size distribution of hydrated slag-blended cement. A partial replacement of ordinary Portland cement (OPC) with BFS modified the mineralogy (especially in the types of C-S-H), resulting in changes to the pore structure. The determined tortuosity and porosity were used in a reactive transport model to predict multi-species transport. Experimentally measured and simulated chloride profiles were in good agreement for hydrated OPC and slag-blended cements exposed to sodium chloride solutions. The causes for the low penetration rate of chloride in slag-blended cementitious materials are discussed considering their pore structure and surface electrical properties. The role of tortuosity on Cl^-/OH^- for the evaluation of chloride induced corrosion was also discussed.

1. Introduction

Cementitious materials are used in low and intermediate radioactive waste disposal facilities (Hostics and Gens 2016). Increased amounts of blended cement consisting blast furnace slag (BFS) or fly ash are expected to see use in such facilities going forward, due to their lower diffusivity and high chemical resistance compared to conventional ordinary Portland cement (OPC) (Niwase *et al.* 2010). Therefore, it has been considered that the use of cementitious materials blended with BFS is an effective method to improve their durability. The durability performance of cementitious materials in service environments is affected by numerous factors, many of which involve attacks due to ionic transport, leading to reduced service life. The durability of cementitious materials must be ensured in both an economically and environmentally responsible manner. In reinforced concrete structures, corrosion of the reinforcing steel is the cause of the most serious durability problems (Malhorta 2000). Extreme environments prompt the ingress of aggressive ions into the concrete and lead to degradation of the concrete structure over time. Accurate estimation of the time it takes for chloride ions to reach the reinforcement is a crucial parameter for estimating the service life of reinforced concrete structures. Chloride penetrates the concrete via adsorption on its surface and further transports to greater depths into the concrete by diffusion (Yu and Page 1991). A number of factors such as porosity, tortuosity, type and amount of hydrates, and characteristics of calcium silicate hydrate (C-S-H) contribute to the concentration of free chloride in the pore solution of concrete for initiating and promoting the corrosion process; these factors have been extensively studied using several different experimental techniques and modeling approaches (Samson and Marchand 2007; Johannesson *et al*. 2007; Hosokawa *et al.* 2011; Glasser *et al*. 2008).

Tortuosity is an important factor for understanding and predicting the diffusion of chloride ions into cementitious materials. It is related to effective diffusivity through either geometric tortuosity or apparent tortuosity which considers both geometric tortuosity and constrictivity, and tortuosity depends on the material morphology (Patel *et al*. 2016). Archie's law has been used previously to fit the tortuosity of cementitious materials, with fitted values of 0.94–4.8 (Yamaguchi *et al*. 2009). Further, Jennings reported a fractal dimension value of 2.73 for the tortuosity (Jennings 2000). A review of the literature shows that it is difficult to directly determine tortuosity in an experimental manner (Ando *et al*. 2015; Kikuchi *et al*. 2009; Nakarai *et al*. 2006; Promentilla *et*

[1]Graduate student, Division of Sustainable Resources Engineering, Faculty of Engineering, Hokkaido University, Sapporo, Japan.
[2]Specially Appointed Associate Professor, Division of Sustainable Resources Engineering, Faculty of Engineering, Hokkaido University, Sapporo, Japan.
*Corresponding author,
E-mail: elakneswaran@eng.hokudai.ac.jp
[3]Associate Professor, Division of Sustainable Resources Engineering, Faculty of Engineering, Hokkaido University, Sapporo, Japan.
[4]Professor, Division of Sustainable Resources Engineering, Faculty of Engineering, Hokkaido University, Sapporo, Japan.

Table 1 Chemical composition and physical properties of raw materials.

	Density (g/cm^3)	Blaine (cm^2/g)	Chemical composition (%)									
			SiO_2	Al_2O_3	Fe_2O_3	CaO	MgO	TiO_2	Na_2O	K_2O	SO_3	Cl
OPC	3.16	3310	21.56	4.68	2.98	65.63	1.3	0.23	0.33	0.33	1.9	0.005
BFS4000	2.91	3930	34.03	14.36	0.83	43.28	6.51	0.46	0.18	0.31		

al. 2009). Different researchers have reported different values for tortuosity obtained using various analytical methods, and hence an appropriate method that considers its physical definition merits the development.

This study proposes a method to determine the tortuosity of hydrated OPC and slag-blended cement from the porosity and diffusivity of C-S-H, predicted by a three-dimensional spatial distribution model proposed previously (Kurumisawa *et al.* 2012). Furthermore, a relationship between the slag replacement ratio and tortuosity was derived. The determined tortuosity values were incorporated into the reactive transport model developed previously (Elakneswaran *et al.* 2010) to predict chloride transport slag-blended cementitious materials. Thermodynamic equilibrium reactions between hydrates and solution, binding of chloride on hydrates (both C-S-H and monosulfate), and the influence of surface charge on multi-species transport were also considered in the reactive transport model in addition to porosity, pore size and tortuosity effects. Finally, the impact of tortuosity on the ratio of chloride to hydroxyl concentration for evaluating the long-term reinforcement corrosion was discussed.

2. Experimental

2.1 Materials and sample preparation

The chemical compositions and physical properties of OPC and BFS are given in **Table 1**. Hydrated cement paste (HCP) was prepared with water to binder ratios (W/B) of 0.3, 0.5, and 0.7, and BFS cement paste (BFSCP) was prepared with a water to binder ratio of 0.5 with BFS replacement ratios of 50% and 70%. Samples were cast in molds (φ50 mm × 100 mm or 40 mm × 40 mm × 160 mm) after mixing and continuous hand-mixing every 30 min to stop bleeding. Samples were sealed for 24 h at room temperature, and then cured in water for 28 or 91 days at 20 °C.

2.2 Backscattered electron image (BEI) and Energy Dispersive X-ray spectrometry (EDX) measurements

Cubes 5 mm in length per side were cut from freeze-dried material after curing, for use in BEI and EDX measurements. Specimens were immersed in epoxy resin under vacuum, and after hardening the resin the specimen surfaces were polished using SiC paper. Polished surfaces were smoothed using 0.25 μm diamond paste, and a Pt layer was applied to provide electric conductivity on the surface. Electron microscopy imaging was conducted under the following conditions: an acceleration voltage of 15 keV, working distance of 17 mm, area size of 200 × 150 μm, and pixel size of 0.32 μm. The resulting resolution in this study was 0.32 μm, and as such pores smaller than 0.32 μm in diameter could not be distinguished. Observations were carried out on 20 areas in each specimen. Unhydrated cement (UH), unhydrated BFS, calcium hydroxide (CH), C-S-H including other hydrates, and pores larger than 0.32 μm in diameter were distinguished using image analysis software and setting brightness thresholds. The average fraction of each phase was considered to be the volume fraction (Igarashi *et al*. 2004). The measured CaO/SiO_2 (C/S) and Al_2O_3/SiO_2 (A/S) ratios of C-S-H are the average of 20 EDX measurements on each specimen. The C/S and A/S were corrected by standard materials (Wollastonite and Jadeite).

2.3 Electron probe microanalyzer (EPMA) measurements

After curing, the cylinder samples were cut into two halves and all surfaces except the cutting face were coated with epoxy resin to ensure chloride penetration in only one direction. The coated samples were exposed to 0.5 mol/l chloride for 28 or 91 days. After exposure, the specimens were cut into two halves parallel to the path of ionic ingress; one part was used for EPMA mapping while the other was used to determine the amount of chloride by a traditional method. An EPMA JEOL JXA-8900M apparatus was used to carry out element mapping. The measurement conditions were as follows: 15 kV accelerating voltage, 50 mA beam current, 60 × 30 μm pixel size, and 1000 × 50 points. The chloride profile was calculated from the mapping, but was expressed as X-ray counts of chloride. The counts were corrected by the determining the chloride concentration from a wet analysis as described in Japanese Industrial Standard (JIS) A 1154. In the wet analysis, powder samples were mixed with 2 M nitric acid solution and boiled for 5 min. The boiled solution was filtered and the concentration of chloride in the solution was measured with ion chromatography.

2.4 Micro-elastic modulus measurements using micro-indentation method

The same specimens which were used for BEI were used here. The elastic moduli of the hydration products were measured using a Fischers scope (HC-100), and 100 indents in a 10 × 10 μm grid were measured in each specimen. The maximum load and speed of the applied load were 20 mN and 1 mN/s respectively. The average value of the measurements in each specimen was determined as the micro elastic modulus of C-S-H.

2.5 Pore size distribution by thermoporometry

Differential scanning calorimetry (DSC) was used to measure the pore size distributions of hydrated samples. For each sample, approximately 28 mg of material was dried at 105 °C for 24 h and immersed in water for 3 h. After immersion, water adhered on the sample surface was wiped off and the samples were placed in an aluminum sample pan. Alumina powder was used as a reference specimen during measurement. The measurement range was 10 °C to -60 °C, and the scanning speed was 2 °C/min. The total moisture content was determined by the weight differences between measurements at 20 and 105 °C. Pore size distribution was determined using a thermoporometry theory reported previously (Brun *et al*. 1977).

2.6 Electric conductivity

Specimen dimensions for electrical conductivity measurements were 40 × 40 × 40 mm. Stainless electrodes (40 × 30 × 0.3 mm) were placed on the specimen 30 mm apart, and the effective area of the electrode was 30 × 30 mm. AC impedance of the specimens was measured over a frequency range of 4 Hz to 5 MHz with an impedance analyzer (HIOKI IM3570) at an applied voltage of 0.1 V. Nyquist plots were established using the measured data, and the bulk resistivity was determined from the point where the electrode resistivity (straight line) and the circle is intersected (Kurumisawa *et al*. 2012), using

$$\rho = \frac{R_a L}{A} \tag{1}$$

$$\sigma = \frac{1}{\rho} \tag{2}$$

where ρ is the bulk resistivity of the specimen, R_a is the measured resistance, L is the distance between electrodes, A is the effective area of the electrode, and σ is the conductivity. The measured electrical conductivity is the normalized conductivity in which the influence of the pore solution is removed by dividing the measured electric conductivity by the pore solution conductivity. The pore solution conductivity was calculated based on hydration degree and the chemical composition of cement (Snyder *et al*. 2003).

3. Modeling approach

3.1 Reactive transport model

An integrated thermodynamic model considering ion–ion and ion–solid interactions was used to simulate multi-ionic transport. The model was implemented in the PHREEQC geochemical code using phase-equilibrium, surface complexation, and multi-component diffusion (MCD) modules. Thermodynamic properties for various phases and minerals present in the cement system were collected from CEMDATA07 (Lothenbach *et al*. 2008) and other sources (Myers *et al*. 2014), and converted into a format suitable for PHREEQC. The converted data, together with the PHREEQC default thermodynamic database (Parkhust and Appelo 1999), were used in this study for each calculation. The details of the integrated thermodynamic model are described elsewhere (Elakneswaran *et al*. 2010).

The diffusive flux of a selected ion, i, considering concentration and electrical potential gradients and the chemical activity effects can be expressed by Nernst-Planck equation as follows (Elakneswaran *et al*. 2010):

$$J_i = -D_{w,i}\left[\frac{\partial \ln(\gamma_i)}{\partial \ln(c_i)}+1\right]\frac{\partial c_i}{\partial x} + D_{w,i} z_i c_i \frac{\sum_{j=1}^{n} D_{w,j} z_j \left[\frac{\partial \ln(\gamma_i)}{\partial \ln(c_j)}+1\right]\frac{\partial c_j}{\partial x}}{\sum_{j=1}^{n} D_{w,j} z_j^2 c_j} \tag{3}$$

where $D_{w,i}$ is its diffusion coefficient, γ_i is its activity coefficient, c_i is its concentration, and z_i is its valance; the subscript j is introduced to show that these species are for the potential term.

The diffusion coefficient of ions in a porous medium, D_p, is related to $D_{w,i}$, porosity, ε, and tortuosity, τ, by Archie's law (Appelo and Postma 2009):

$$D_p = D_{w,i}\varepsilon_w^{\tau} \tag{4}$$

3.2 Three-dimensional spatial distribution model

3.2.1 Autocorrelation function calculations

To reconstruct a three-dimensional spatial image of the hardened cement paste, the autocorrelation function (ACF) was used for different phases (UH, CH, pores, slag and other phases) to generate a binary image from BEI without the C–S–H phase, which was not included because it is the matrix and acts as a continuous phase in the hardened cement paste. The ACF is a two-point correlation function, defined as the probability that two arbitrary points are in the same phase as a function of the distance between them (Torquato 2001). Thus, the position of each phase can be determined using ACF. The following procedure was used for calculating ACF in this study (Bentz 2000). The summation of $S(x,y)$ was determined for an $M \times N$ image using the following equation:

$$S(x,y) = \sum_{i=1}^{M-x}\sum_{j=1}^{N-y}\frac{I(i,j)\times I(i+x,j+y)}{(M-x)(N-y)} \tag{5}$$

where $I(x,y)$ is 1 if the pixel at location (x,y) contains the phase(s) of interest, and is 0 otherwise. $S(x,y)$ is then converted into the $S(r)$ function for the distance r between pixels using bilinear interpolation of $S(x,y)$ values as follows:

$$S(r) = \frac{1}{2r+1}\sum_{l=0}^{2r} S\left(r, \frac{\pi l}{4r}\right) \tag{6}$$

3.2.2 Three-dimensional spatial image reconstruction

ACF $S(r)$ was used to reconstruct a three-dimensional image of the microstructure for each phase. Pixels in the three-dimensional spatial image are assigned random numbers with a normal distribution of $N(x, y, z)$, generated using the Box–Muller method (Bentz and Garboczi 1991). This random number distribution of $N(x, y, z)$ is modified using a filter function $F(x, y, z)$ using the ACF $S(r)$. Finally, the resultant image $R(x, y, z)$ is generated using the following equation:

$$R(x,y,z)=\sum_{i=0}^{30}\sum_{j=0}^{30}\sum_{k=0}^{30}N(x+i,y+j,z+k)*F(i,j,k) \quad (7)$$

where $F(x,y,z)$ is determined as

$$F(r)=F(x,y,z)=\frac{\left[S(r=\sqrt{x^2+y^2+z^2})-S(0)\times S(0)\right]}{\left[S(0)-S(0)\times S(0)\right]} \quad (8)$$

The threshold operation was carried out to obtain appropriate volume fractions in regards to the pixels in $R(x, y, z)$, which were originally assigned to the respective phases of interest (UH, pores, BFS, or CH). For example, if a value of $R(x, y, z)$ is larger than the critical threshold, the pixel is assigned to the phase of interest; otherwise, it is assigned to the original phase. The reassigned number of pixels corresponds to measured volume fraction using the BEI. The reconstructed size of the image is 100^3 voxels where one voxel is equivalent to 0.32 μm^3 according to the BEI observations. Three different images with different random numbers were reconstructed to confirm the reproducibility of the model; periodic conditions were also applied to all faces.

An outline of the 3D spatial reconstruction model is illustrated in **Fig. 1**. The area fraction of each phase was calculated from scanning electron microscopy (SEM) images, and 3D-spatial distribution models from the calculated area functions. Finally, the diffusivity of C-S-H was derived from this model as electrical conductivity. In this model, the input parameter is the diffusivity of C-S-H and the capillary pore, and the output parameter is diffusivity of a given specimen; this analysis is described further in section 4.3.

4. Results and discussion

4.1 CaO/SiO_2, Al_2O_3/SiO_2 ratios and BEI

The CaO/SiO_2 (C/S) and Al_2O_3/SiO_2 (A/S) ratios of BFSCP are shown in **Fig. 2** as functions of the slag replacement ratio. The A/S ratio increases while the C/S ratio decreases with increasing BFS replacement ratio,

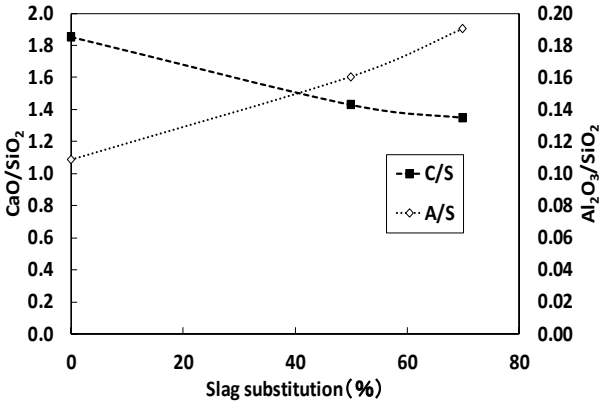


Fig. 2 CaO/SiO_2 and Al_2O_3/SiO_2 ratios as functions of slag replacement ratio.

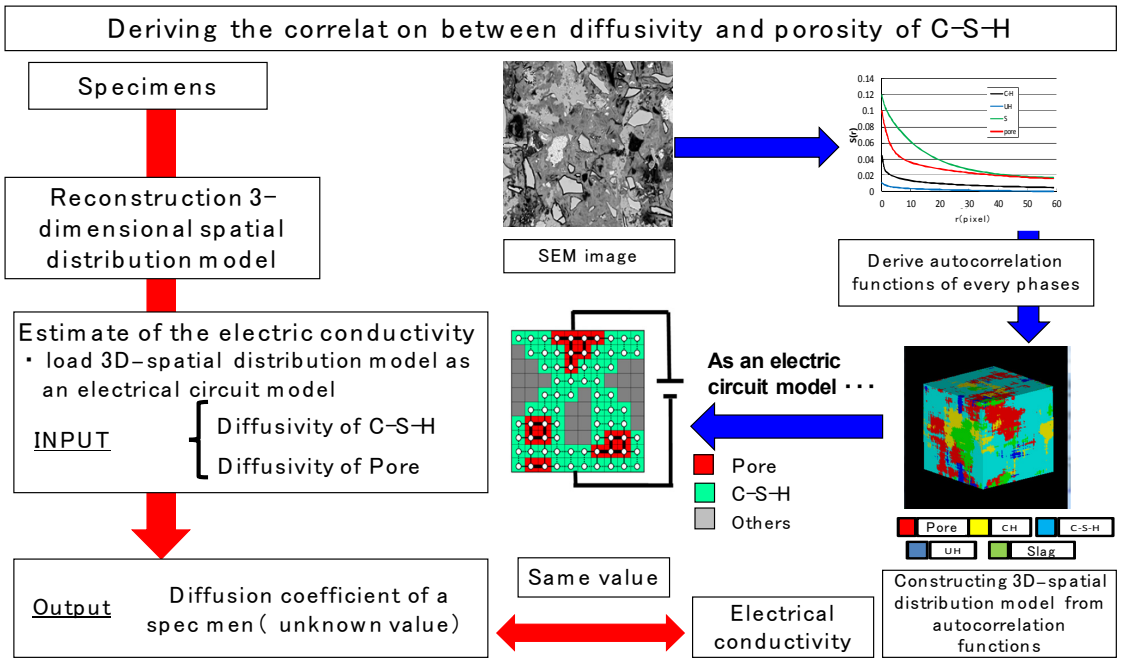


Fig. 1 Procedures for deriving the relationship between the diffusivity and porosity of C-S-H.

which is consistent with previous reports (Taylor *et al.* 2010). Some of the silica in C-S-H is substituted by aluminum to form C-A-S-H in slag-blended cement. The A/S ratio also increases as Al_2O_3 increases with slag addition. The experimental results show the presence of aluminum in the C-S-H of HCP as reported in previous studies (Lothenbach *et al.* 2011; Kocaba 2009). These ratios modify the structure of C-S-H/C-A-S-H and can affect the durability performance of concrete. BEIs of HCP and BFSCP of 50% and 70% replacement after 91 days of curing are shown in **Fig. 3**. Unreacted BFS is still present in the sample after 91 days of curing. In this study, BEIs were separated into five phases based on brightness: pores are black, calcium hydroxide is dark gray, C-S-H is light gray, unhydrated cement is white and unreacted BFS is bright white. The area fraction of each phase as determined by BEI experiments is shown in **Fig. 4**. As the hydration progress, the amount of hydration products increase, and the pore and un-hydrated cement and slag decrease. The increase of calcium hydroxide in BFSCP with hydration time is observed in the figure. This might be due to different in the hydra-

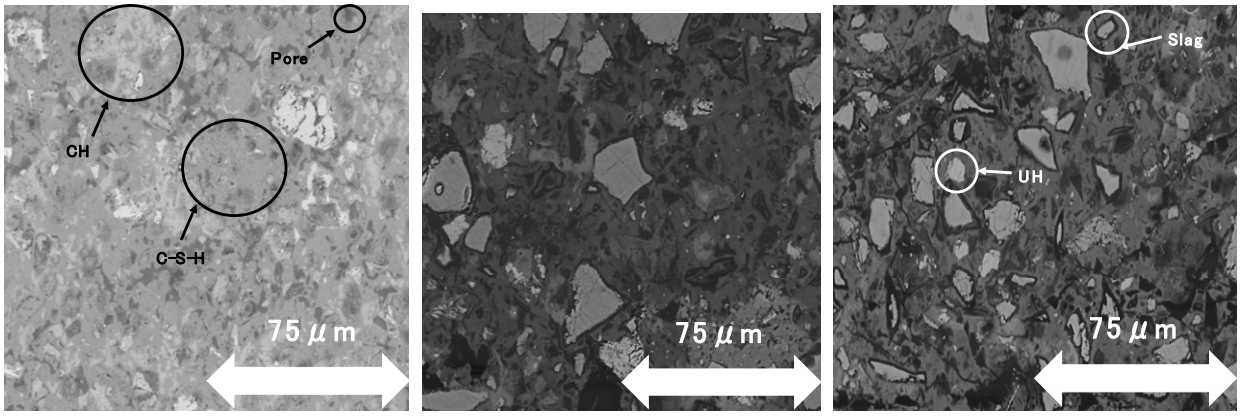


Fig. 3 Backscattered electron images of HCP (left), and BFSCPs of 50% (center) and 70% replacement (right).

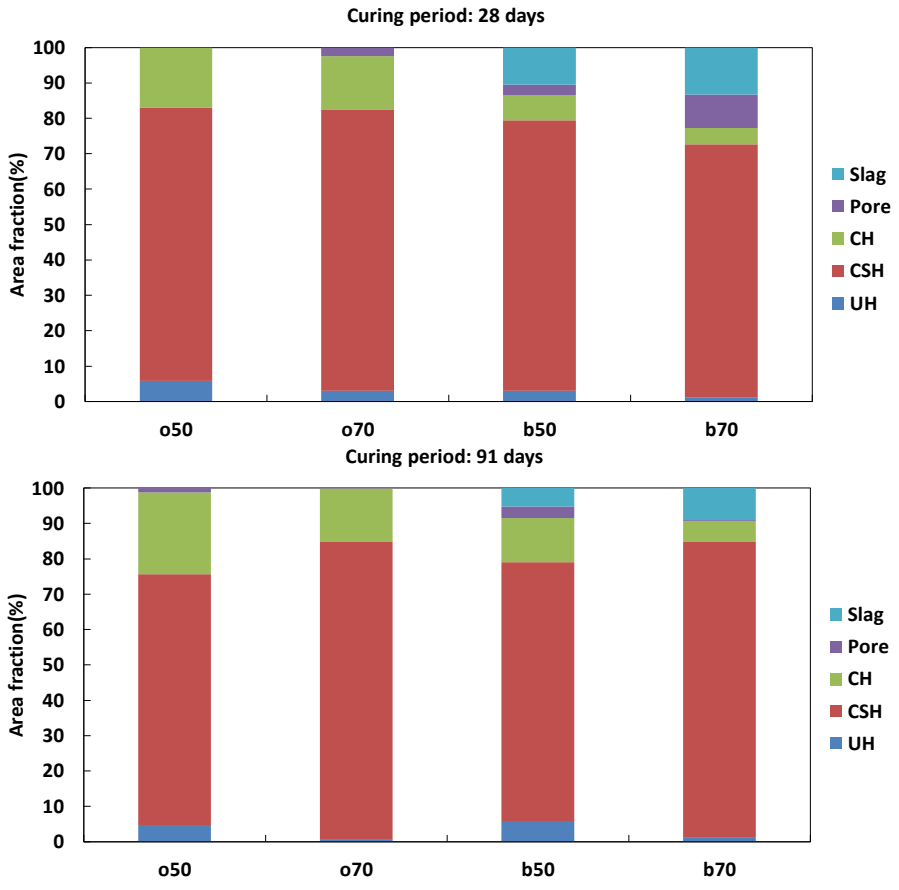


Fig. 4 Area fractions determined by BEI experiments. Notation: o50: OPC-W/B (%); b50: BFS-percentage of slag replacement (W/B=0.5).

tion degree; hydration of cement is higher than that of slag in this study. The amount of calcium hydroxide will not affect the other calculation results because C-S-H dominates the volume of hydration products. Three-dimensional spatial image models were reconstructed based on an autocorrelation function (described in section 3.2) derived from these backscattered electron images.

4.2 Electrical conductivity

The results of electrical conductivity measurements of HCP and BFSCP are shown in **Fig. 5**. The electric conductivity of each specimen decreases with increasing BFS replacement ratio for each W/B, and decreases with decreasing W/B. The electrical conductivity of cementitious materials generally depends on porosity, pore connectivity and pore solution conductivity. The influence of W/B on the electrical conductivity is linked to changes in porosity: decreasing W/B decreases the porosity and thus lowers the electrical conductivity due to limited paths for ionic movement. The electrical conductivity of the pore solution becomes significant when the specimens have the same porosity. Pore solution concentration (especially in regards to sodium and potassium ions) decrease with BFS replacement ratio, reducing the conductivity.

4.3 Determination of tortuosity from diffusivity and porosity of C-S-H

The porosity of C-S-H can be determined by the relationship between its elastic modulus and porosity (Jennings *et al*. 2007),

$$\varphi_{C-S-H} = 0.5 - 0.0077 \times E_{micro} \quad (9)$$

where φ_{C-S-H} is the porosity of C-S-H and E_{micro} is the elastic modulus of C-S-H. The median value of the elastic modulus of hydrated cement and slag specimens, determined by a micro-indentation method, is considered as the elastic modulus of C-S-H because it is the major phase (> 70% in volume). The results of the elastic modulus and calculated porosity of C-S-H are shown in **Fig. 6**.

The reconstructed three-dimensional spatial images were used to calculate the diffusion coefficient of HCP and BFSCP based on the model proposed by Garboczi and Bohn (2003). The diffusivity in a steady state condition, as with conductivity, can be predicted by express-

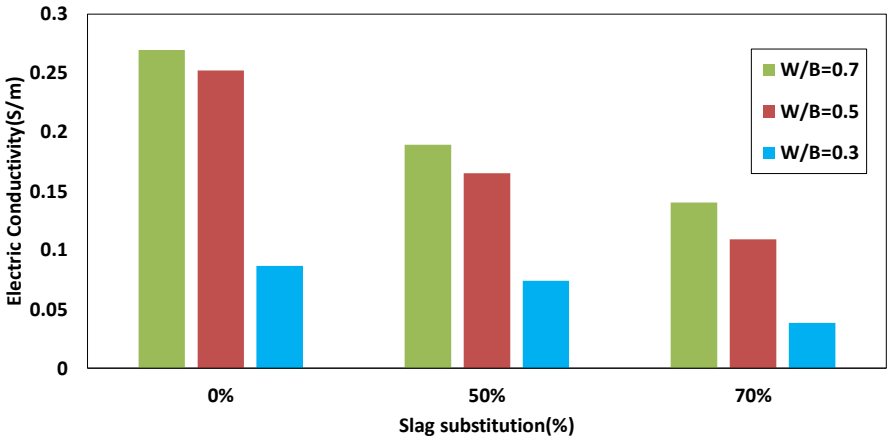


Fig. 5 Electric conductivity of HCP and BFSCP cured for 28 days.

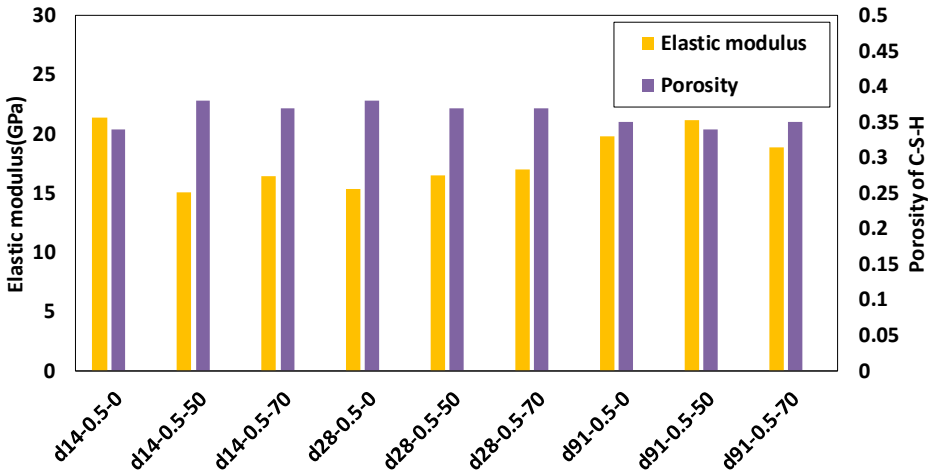


Fig. 6 Elastic modulus and porosity of C-S-H. Notation: dx-y-z: curing period-W/B-slag replacement ratio.

ing it in the following Nernst-Einstein relation:

$$\frac{D}{D_0}=\frac{\sigma}{\sigma_0} \tag{10}$$

where D is the measured diffusivity, D_0 is the diffusivity of the ions in free water, σ is then measured electrical conductivity and σ_0 is the conductivity of the pore solution.

In this model, the diffusivity of the capillary pore and C-S-H are necessary for estimating the diffusivity of the overall material. The diffusion coefficient of chloride ions in the capillary pores was held at 1.81×10^{-9} (m^2/s) (Jensen *et al*. 1999). The diffusion coefficient of the C-S-H, the unknown parameter, was calculated based on the electric conductivity results given in **Fig. 5**. The relationship between the diffusion coefficient and porosity of C-S-H is shown in **Fig. 7**. In addition to the specimens considered in **Fig. 6**, HCP specimens prepared at W/B of 0.3 and 0.7 cured for 28 and 91 days and BFSCP specimens prepared at W/B of 0.4 and cured for 28 days were considered to determine diffusivity of C-S-H.

As shown in **Fig. 7**, the diffusion coefficient of C-S-H decreases with the slag replacement ratio in accordance with reported studies (Kurumisawa *et al*. 2012). The relationship between the diffusion coefficient and the porosity of C-S-H can be fitted to Archie's law (Eq. (4)) as follows for each slag replacement ratio to determine the tortuosity:

BFS replacement ratio of 0% :

$$D_{C-S-H}=1.0\times1.0^{-9}\cdot\varphi^{2.3892} \tag{11}$$

BFS replacement ratio of 50% :

$$D_{C-S-H}=1.0\times1.0^{-9}\cdot\varphi^{2.6314} \tag{12}$$

BFS replacement ratio of 70% :

$$D_{C-S-H}=1.0\times1.0^{-9}\cdot\varphi^{2.8457} \tag{13}$$

where D_{C-S-H} is the diffusion coefficient of C-S-H and φ is the porosity of C-S-H. A value of 1.0×10^{-9} (m^2/s) was assumed for the diffusion coefficient of ions in free water for best fit, considering the multi-species in the pore solution of hydrated cement and slag which typically has a self-diffusion coefficient of 0.6 to 1.81×10^{-9} (m^2/s). The determined tortuosity can be related to slag replacement ratio, r_{sg}, as:

$$\tau=0.63r_{sg}+2.37 \tag{14}$$

This relationship is plotted in **Fig. 8**. The increase in

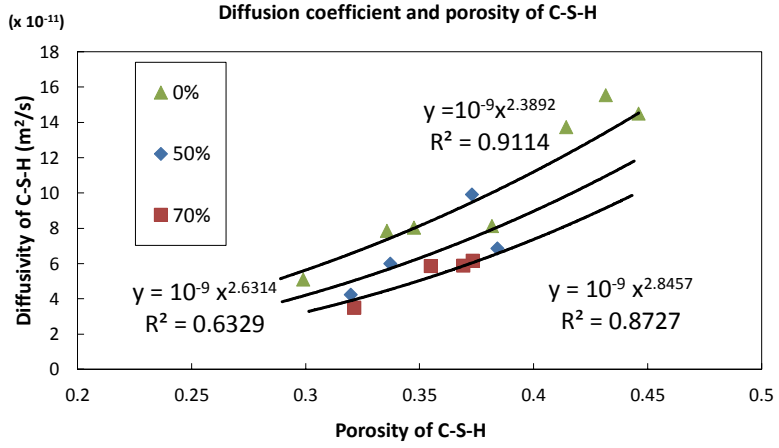


Fig. 7 Relationship between diffusion coefficient and porosity of C-S-H.

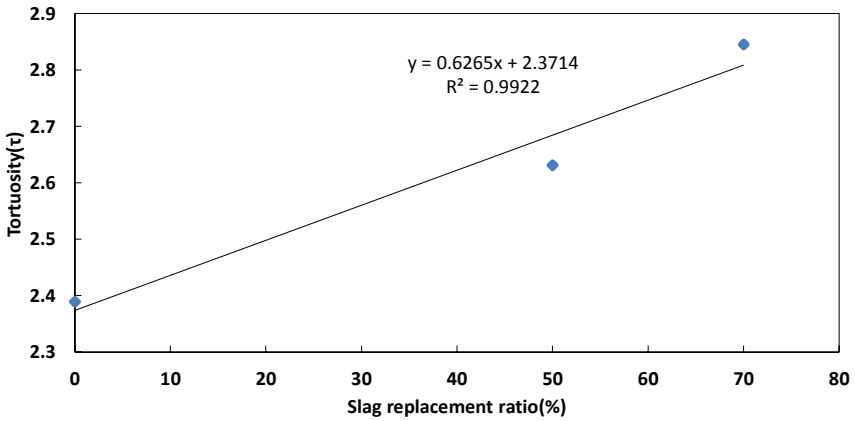


Fig. 8 Relationship between tortuosity and slag replacement ratio.

tortuosity with slag replacement ratio indicates that the diffusion path of chloride ions becomes more complex as more slag is added. The estimated tortuosity values agree reasonably well with values reported in previous studies (Jennings 2000).

4.4 Pore structure

The pore size distributions of HCP and BFSCP as determined by thermoporometry (28 and 91 days curing) are shown in **Fig. 9**. As assumed in a previous study (Jennings 2008), pores are classified as one of two types: small gel pores (< 5 nm) and large gel pores (5–10 nm). The number of small gel pores increases with the BFS replacement ratio, and the amount of large gel pores increases as the water to powder ratio increases. This is related to the pores in the different C-S-H phases: low-density C-S-H (LD C-S-H) and high-density C-S-H (HD C-S-H) (Tennis and Jennings 2000). LD C-S-H consists of large gel pores while HD C-S-H has small gel pores. Therefore, a large amount of LD C-S-H is formed at high W/B, and slag addition leads to the formation of HD C-S-H. Overall, the number of pores decreases and they become smaller with curing period increases. The characteristics of HD C-S-H and LD C-S-H are respectively similar to that of the inner- and outer-products of hydrating cement and/or slag due to their porosity (Maekawa *et al*. 2003). Their microstructure and properties can influence ionic diffusion through cementitious materials. The measured total porosity is used in the prediction of chloride ions diffusion.

4.5 Comparison between measured and estimated chloride ingress

One-dimensional numerical analysis was performed to simulate cylindrical samples of HCP and BFSCP (50 mm diameter, 50 mm height) exposed to 1 L of 0.5 M NaCl solution for 28 and 91 days. Multi-species transport was performed considering common ions such as Na^+, Cl^-, K^+, SO_4^{2-}, Ca^{2+}, Al^{3+}, Si^{4+} and OH^-. Self-diffusion coefficients of ions in free water for a specified temperature were used as diffusion coefficients. In the simulations, the initial and final boundary conditions were set to 0.5 M NaCl and zero flux, respectively. The pore solution concentration and the amount of hydrates required for the simulations were calculated based on a hydration model reported previously (Elakneswaran *et al*. 2016). Although capillary pores are included in the diffusion path of chloride ions, it is considered that chloride diffusion is controlled by C-S-H because the amount of C-S-H is more than 70% in volume of specimen from the result of BEI as shown in **Fig. 4**. The chloride ions diffuse through a series of pores having

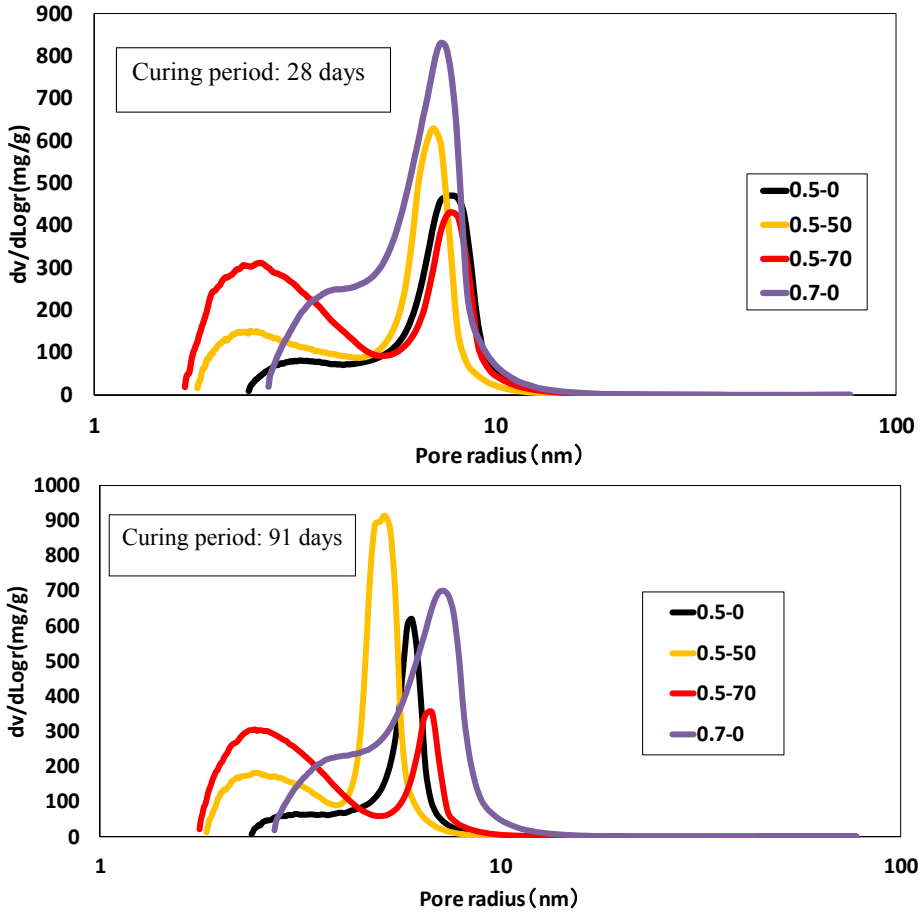


Fig. 9 Pore size distribution of HCP and BFSCP. Notation: W/B-slag replacement ratio.

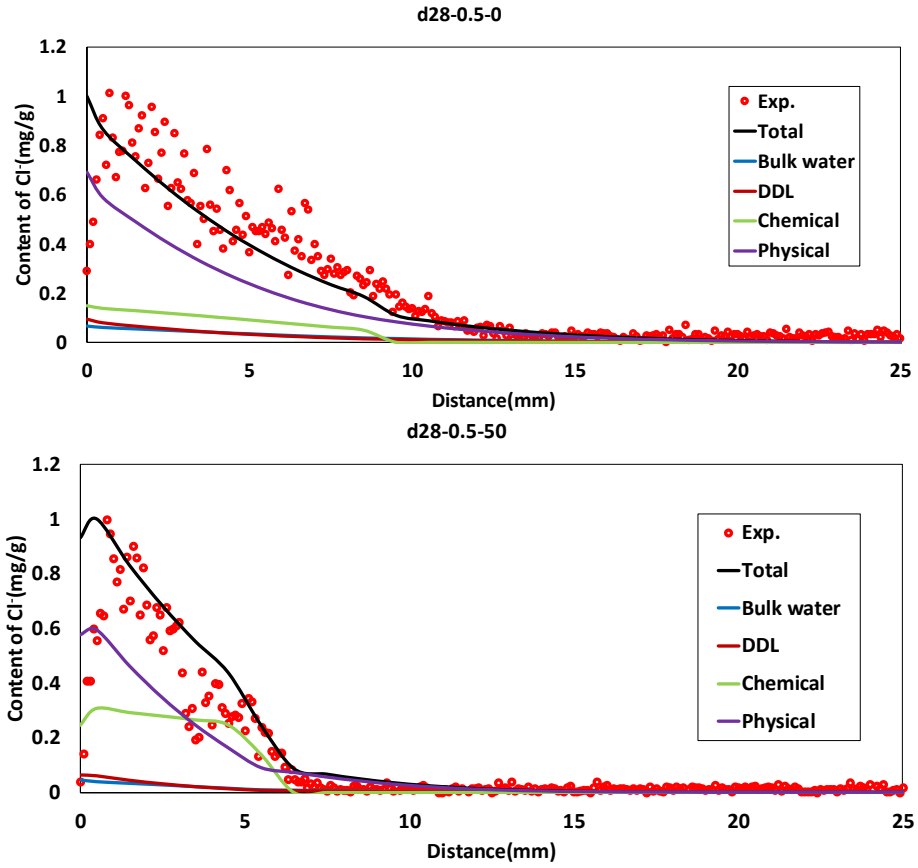
Table 2 Porosity, tortuosity, and pore radius used in simulations.

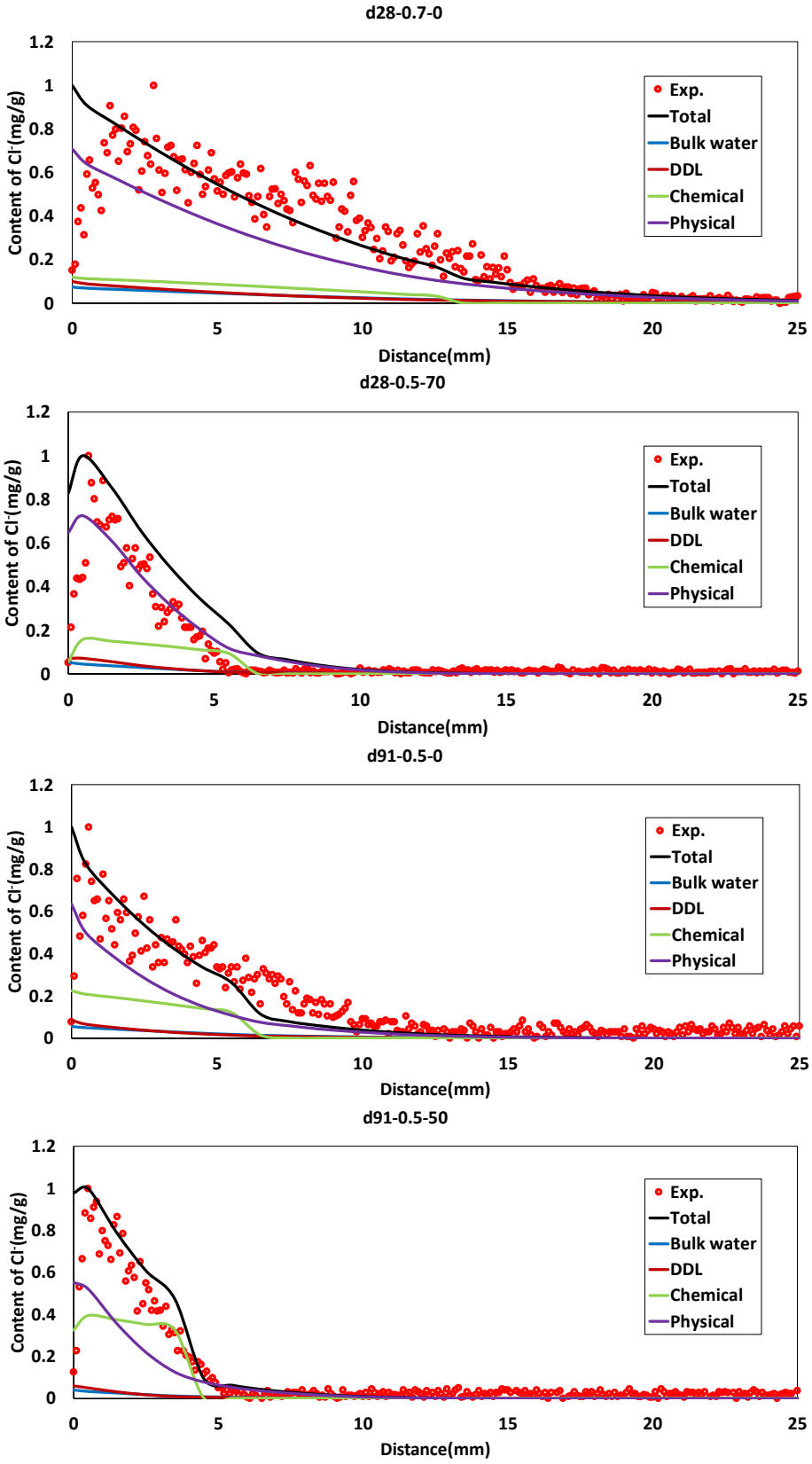
Curing period: 28 days			
W/B-slag replacement ratio	Porosity	Tortuosity	Pore radius (nm)
0.5-0	0.245	2.39	3.2
0.5-50	0.253	2.63	2.3
0.5-70	0.259	2.85	2.1
0.7-0	0.332	2.39	3.4
Curing period: 91 days			
0.5-0	0.200	2.39	3.2
0.5-50	0.214	2.63	2.3
0.5-70	0.226	2.85	2.1
0.7-0	0.311	2.39	3.4

various diameter. A cylindrical pore shape having a single size was assumed for the diffusion, which plays a critical influence on the ionic diffusion. The size of the critical pore was assumed based on the pore size distribution and the surface areas of C-S-H. The pore consists of free water and diffuse double layer, and the volume of free water is used to calculate surface area. The other necessary input parameters such as porosity (from thermoporometry measurements), tortuosity (calculated in section 4.3), and assumed pore radius are tabulated in **Table 2**.

Figure 10 compares the calculated and experimental total chloride profiles. The predicted amounts of chloride in the free water of the pore solution, diffuse double layer, chemically bound as Friedel's salt, and adsorbed on C-S-H surface are also presented. Although several different mechanisms are present, the physical adsorption of chloride dominates total, which supports previous experimental studies in blended cements (Saeki and Sasaki 2006). The presence of AFm phases, which is more pronounced in slag-blended cements than conventional Portland cements, contributes to the chemical binding of chloride. BFSCP shows lower penetration rates than those of HCP over both exposure periods due to changes to the mineralogy and pore structure as more slag is added. Furthermore, high addition of slag leads to better resistance for chloride transport.

The calculated tortuosity suggests that the diffusion path of BFSCP is longer than that of HCP. Hydration of cement and slag, and the associated microstructure development mechanisms proposed by Maekawa and associates (Maekawa *et al*. 2003; Luan *et al*. 2012), were considered here to propose a chloride diffusion path (**Fig. 11**). Ionic diffusion occurs in the pores of both the inner and outer products, and threshold pores or bottleneck exists in the inner products. The pores in the inner products are very small in size, and would be completely covered by the electrical double layer (EDL). 5 nm radius pores are fully filled EDL in HCP (Elakneswaran *et al*. 2010), but this size dimension is larger in BFSCP because of the lower ionic strength of the pore solution compared to HCP. Ionic diffusion through the pores of outer products has less effect from surface charge of C-S-H, but the diffusion is greatly affected by




d28-0.7-0
Content of Cl-(mg/g)
Distance(mm)
Exp.
Total
Bulk water
DDL
Chemical
Physical
d28-0.5-70
Content of Cl-(mg/g)
Distance(mm)
Exp.
Total
Bulk water
DDL
Chemical
Physical
d91-0.5-0
Content of Cl-(mg/g)
Distance(mm)
Exp.
Total
Bulk water
DDL
Chemical
Physical
d91-0.5-50
Content of Cl-(mg/g)
Distance(mm)
Exp.
Total
Bulk water
DDL
Chemical
Physical

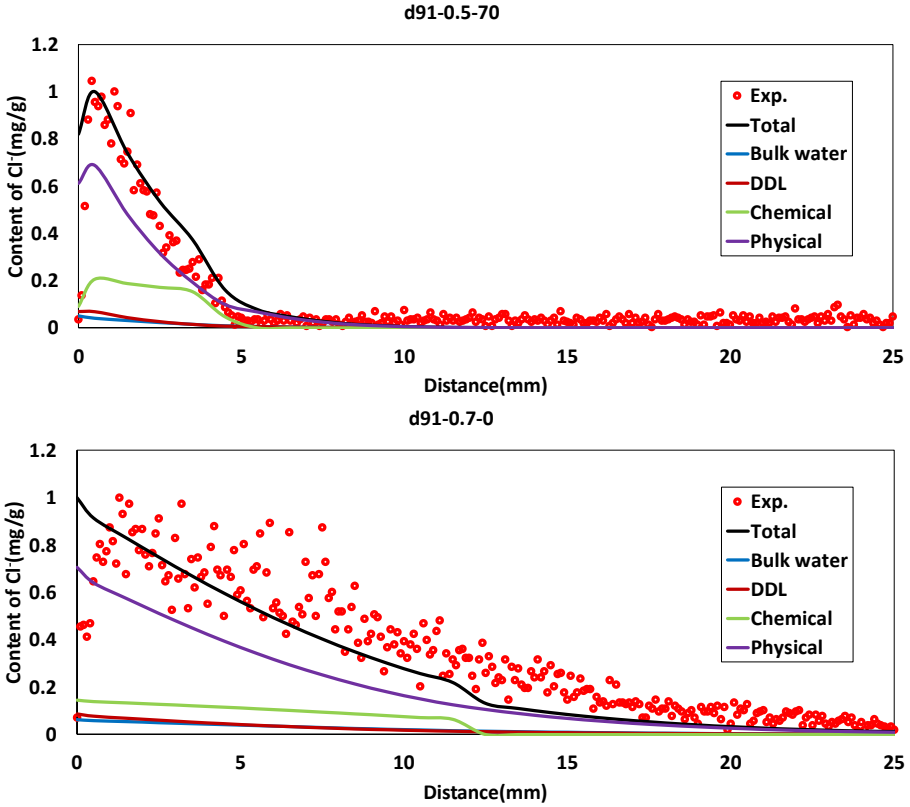


Fig. 10 Comparison between measured and simulated chloride profiles for HCP and BFSCP after 28 and 91 days of 0.5 M NaCl exposure. Notation: dx-y-z: curing period-W/B-slag replacement ratio; Exp.: Experimentally measured total Cl^-; Total: Predicted total Cl^-; Bulk water: Predicted free Cl^- in bulk pore water; DDL: Predicted free Cl^- in diffuse double layer; Chemical: Predicted chemically bound Cl^-; Physical: Predicted physically adsorbed Cl^- on C-S-H.

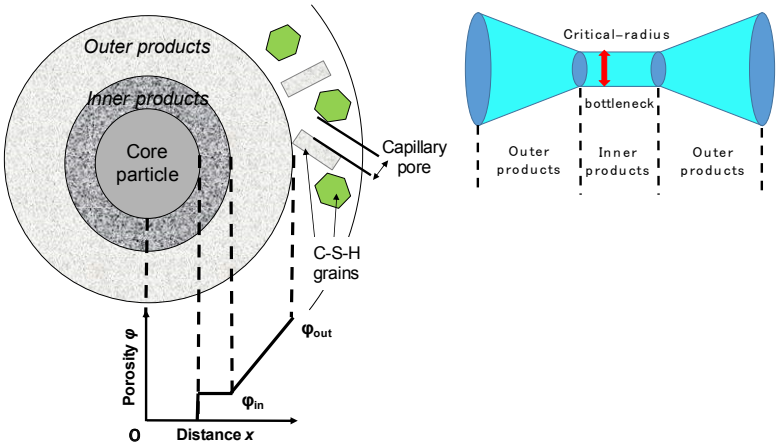


Fig. 11 Concept of ionic diffusion path considering tortuosity and bottleneck pores.

surface charge in the pore of inner products. When the pores of the outer and inner products are connected (**Fig. 11**), diffusion through the inner products controls the overall diffusion rate. This is significant in slag-blended cement due to having large EDL thickness, high tortuosity, and small threshold pore size, which change with the slag replacement ratio to promote a lower penetration rate.

4.6 Simulation results on evaluation of reinforcement corrosion

The Cl^-/OH^- ratio is a useful parameter for evaluating reinforcement corrosion in concrete structures. For Cl^-/OH^- ratio, Cl^- is the summation of the total chloride concentration in free solution and in the diffuse double layer, and OH^- was calculated based on the pore solution pH. The threshold value of Cl^-/OH^- to initiate corrosion is 3–5 (Kari *et al*. 2013). The impact of slag addition on the ratio at a depth of 45 mm as a function of exposure

period is presented in **Fig. 12**. Input parameters for the simulations are the same as described in section 4.5. Slag-blended cement shows better performance against chloride-induced corrosion than Portland cement. Corrosion initiation for a Cl^-/OH^- ratio of 3.0 in slag-blended cement is 10 years longer than that of OPC, and the reinforcement in OPC starts to corrode after 30 years for a threshold ratio of 5.0; slag-blended cement serves more than 100 years under similar conditions. Another simulation was performed to evaluate the impact of tortuosity on the Cl^-/OH^- ratio. The simulation results of Cl^-/OH^- ratio at a depth of 45 mm for OPC are shown in **Fig. 13**. Higher tortuosity leads to a low Cl^-/OH^- ratio and longer service life of the concrete against chloride attack as a result. This is remarkable for a tortuosity value of 3.5. The simulation results show that a partial substitution of OPC by slag, in combination with increasing tortuosity, are important factors to reduce Cl^-/OH^- ratio as pertains to chloride induced corrosion. As such, these factors should be considered in the material design of concrete structures exposed to chloride-rich environments.

5. Conclusions

The tortuosity of hydrated cementitious materials blended with slag was determined by fitting the porosity and diffusivity of C-S-H, predicted through a three-dimensional spatial distribution model, to Archie's law. The determined tortuosity is linearly related to the slag replacement ratio which indicates that ionic diffusion path becomes longer after a partial replacement of OPC with slag. Hydration of cement and slag forms LD C-S-H and HD C-S-H, and the associated pores are small gel pores (< 5 nm) in HD C-S-H and large gel pores in LD C-S-H. The amount of the small and large pores depends on W/B, slag addition, and curing period; large gel pores form at high W/B, and slag addition creates more small gel pores. The chloride profiles predicted using the determined tortuosity and porosity agree well with the measured profiles for both HCP and BFSCP exposed to 0.5 M NaCl solution for 28 and 91 days, predicted physical adsorption of chloride controls the total. The addition of slag leads to large EDL thickness, high tortuosity, and small threshold pore size which shows high chloride penetration resistance in slag-blended cementitious materials. The simulation results on Cl^-/OH^-, an indicator for evaluating the chloride induced corrosion, show that high durability of reinforced concrete can be achieved with slag addition and increased tortuosity values.

Acknowledgements

This study was financially supported by JSPS KAKENHI Grant No:16K1812906 and 16K0656306. A part of this study was conducted at the Joint-use Facili-

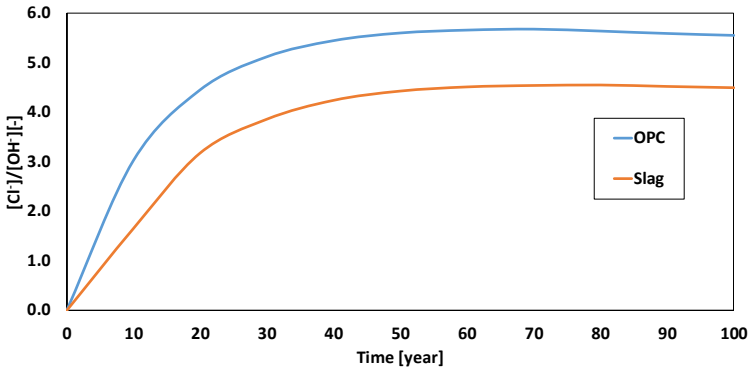


Fig. 12 Cl^-/OH^- ratio at a depth of 45 mm as a function of exposure time for hydrated OPC and slag-blended cement exposed to 0.5 M NaCl.

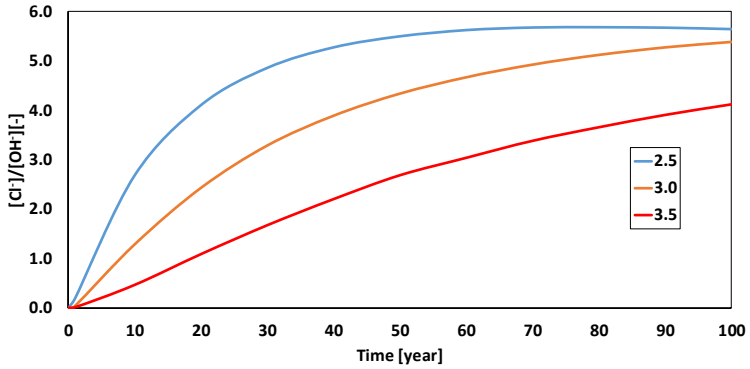


Fig.13 Cl-/OH- ratio at a depth of 45 mm as a function of exposure time for hydrated OPC with different tortuosity values exposed to 0.5 M NaCl.

ties: Laboratory of Nano-Micro Material Analysis at Hokkaido University, supported by the Nanotechnology Platform Program of the Ministry of Education, Culture, Sports, Science and Technology (MEXT), Japan.

References

Ando, M., Kobayashi, H., Uenaka, S. and Nawa, T., (2015). "Quantification of tortuosity of pore network for diffusion of chloride ion transport into hardened cement paste." *Cement Science and Concrete Technology*, 69, 96-103. (in Japanese)

Appelo, C. A. J. and Postma, D., (2009). "*Geochemistry, groundwater and pollution*." CRC Press Taylor & Francis Group.

Bentz, D. P., (2000) "CEMHYD3D: A three-dimensional cement hydration and microstructure development modelling package version 2.0." NISTIR 648

Bentz, D. P. and Garboczi, E. J., (1991). "Percolation of phases in a three-dimensional cement paste microstructural model." *Cement and Concrete Research,* 21(2-3), 325-344.

Bohn, R. B. and Garboczi, E. J., (2003). "*User Manual for Finite Element and Finite Difference Programs:* A Parallel Version of NIST IR 6269."

Brun, M., Lallemand, A., Quinson, J. F. and Eyraud, C., (1977). "A new method for the simultaneous determination of the size and shape of pores: The thermoporometry." *Thermochimica Acta*, 21(1), 59-88.

Elakneswaran, Y., Iwasa, A., Nawa, T. and Kurumisawa, K., (2010). "Ion-cement hydrates interactions govern multi-ionic transport model for cementitious materials." *Cement and Concrete Research*, 40, 1756-1765.

Elakneswaran, Y., Owaki, E., Miyahara, S., Ogino, M., Maruya, T. and Nawa, T., (2016). "Hydration study of slag-blended cement based on thermodynamic considerations." *Construction and Building Materials,* 124, 615-625.

Glasser, F. P., Marchand, J. and Samson, E., (2008). "Durability of concrete - degradation phenomena involving detrimental chemical reactions." *Cement and Concrete Research*, 38(2), 226-246.

Hosokawa, Y., Yamada, K., Johanneson, B. and Nilsson, L.-O., (2011). "Development of a multi-species mass transport model for concrete with account to thermodynamic phase equilibrium." *Materials and Structures*, 44, 1577-1592.

Hostics, V. L. and Gens, R., (2016). "*Performance assessment of concrete structures and engineered barriers for nuclear applications - Conclusions of RILEM TC226-CNM*." Springer Nature.

Igarashi, S., Kawamura, M. and Watanabe, A., (2004). "Analysis of cement pastes and mortars by a combination of backscatter-based SEM image analysis and calculations based on the Powers model." *Cement and Concrete Composites*, 26(8), 977-985.

Jennings, H. M., (2000). "Model for the microstructure of calcium silicate hydrate in cement paste." *Cement and Concrete Research*, 30(1), 101-116.

Jennings, H. M., (2008). "Refinements to colloid model of C-S-H in cement: CM-II." *Cement and Concrete Research*, 38, 275-289.

Jennings, H. M., Thomas, J. J., Gevrenov, J., Constantinides, G. and Ulm, F.-J., (2007). "A multi-technique investigation of the nanoporosity of cement paste." *Cement and Concrete Research*, 37(3), 329-336.

Jensen, O. M., Freiesleben Hansen, P., Coats, A. M. and Glasser, F. P., (1999). "Chloride ingress in cement paste and mortar." *Cement and Concrete Research*, 29 (9), 1497-1504.

Johannesson, B., Yamada, K., Nilsson, L.-O. and Hosokawa, Y., (2007). "Multi-species ionic diffusion in concrete with account into interaction between ions in the pore solution and the cement hydrates." *Materials and Structures*, 40(7), 651-665.

Kari, O. P., Elakneswaran, Y., Nawa, T. and Puttonen, J., (2013). "A model for a long-term diffusion of multispecies in concrete based on ion-cement-hydrate interaction." *Journal of Materials Science*, 48(12), 4243-4249.

Kikuchi, M., Sasaki, K., Suda, Y. and Saeki, T., (2009). "Effect of chemical composition of C-S-H on chloride diffusion." *Cement Science and Concrete Technology*, 63, 354-361. (in Japanese)

Kocaba, V., (2009), "*Development and evaluation of methods to follow microstructural development of cementitious systems including slags*." Thesis (PhD). École Polytechnique Fédérale de Lausanne.

Kurumisawa, K., Nawa, T. and Owada, H., (2012). "Prediction of the diffusivity of cement-based materials using a three-dimensional spatial distribution model." *Cement and Concrete Composites*, 34(3), 408-418.

Lothenbach, B., Matschei, T., Möschner, G. and Glasser, F. P.,(2008). "Thermodynamic modelling of the effect of temperature on the hydration and porosity of portland cement." *Cement and Concrete Research*, 38 (1), 1-18.

Lothenbach, B., Scrivener, K. and Hooton, R. D., (2011). "Supplementary cementitious materials." *Cement and Concrete Research*, 41(12), 1244-1256.

Luan, Y., Ishida, T., Nawa, T. and Sagawa, T., (2012). "Enhanced Model and Simulation of Hydration Process of Blast Furnace Slag in Blended Cement." *Journal of Advanced Concrete Technology*, 10(1), 1-13.

Maekawa, K., Ishida, T. and Kishi, T., (2003). "Multi-scale modeling of concrete performance." *Journal of Advanced Concrete Technology*, 1(2), 91-126.

Malhorta, V., (2000) "*Durability of concrete.*" In: R. W. Revie (Ed) *Corrosion*, Wiley.

Myers, R. J., Bernal, S. A. and Provis, J. L., (2014). "A

thermodynamic model for C-(N-)A-S-H Gel: CNASH_ss. Derivation and validation." *Cement and Concrete Research*, 66, 27-47.

Nakarai, K., Ishida, T. and Maekawa, K., (2006). "Multi-phase physicochemical modeling of soil-cementitious material interaction." *Soils and Foundations*, 46(5), 653-663.

Niwase, K., Naoyuki, S. and Tsuji, Y., (2010). "Materials and proportion's design of self-compacting mortar used for low diffusion layer in sub-surface radioactive waste disposal facility in Japan." *Cement Research and Technology*, 3, 43-51. (in Japanese)

Parkhust, D. L. and Appelo, C. A. J., (1999). "*A computer program for speciation, batch-reaction, one- dimensional transport and inverse geochemical calculations*." USGS report.

Patel, R. A., Phung, O. T., Seetharam, S. C., Perko, J., Jacques, D., Naes, N., De Schutter, G., Ye, G. and van Breugel, K., (2016). "Diffusivity of saturated ordinary portland cement-based materials: A critical review of experimental and analytical modelling approaches." *Cement and Concrete Research*, 90, 52-72.

Promentilla, M. A. B., Sugiyama, T., Hitomi, T. and Takeda, N., (2009). "Quantification of tortuosity in hardened cement pastes using synchrotron-based X-Ray computed microtomography." *Cement and Concrete Research*, 39(6), 548-557.

Saeki, T. and Sasaki, K., (2006). "Chloride binding capacity of calcium silicate hydrate." *Cement Science and Concrete Technology*, 60, 322-327. (in Japanese)

Samson, E. and Marchand, J., (2007). Modelling the transport of ions in unsaturated cement-based materials." *Computer & Structures*, 85, 1740-1756

Snyder, K. A., Feng, X., Keen, B. D. and Mason, T. O., (2003). "Estimating the electrical conductivity of cement paste pore solutions from OH^-, K^+ and Na^+ concentrations." *Cement and Concrete Research*, 33(6), 793-798.

Taylor, R., Richardson, I. G. and Brydson, R. M. D., (2010). "Composition and microstructure of 20-year-old ordinary portland cement-ground granulated blast-furnace slag blends containing 0 to 100% slag." *Cement and Concrete Research*, 40(7), 971-983.

Tennis, P. D. and Jennings, H. M., (2000). "Model for two types of calcium silicate hydrate in the microstructure of portland cement pastes." *Cement and Concrete Research*, 30(6), 855-863.

Torquato, S., (2001). "*Random heterogeneous materials: Microstructure and macroscopic properties*." Springer.

Yamaguchi, T., Negishi, K. and Hoshino, S., (2009). "Modeling of diffusive mass transport in micropores in cement based materials." *Cement and Concrete Research*, 39(12), 1149-1155.

Yu, S. W. and Page C. L., (1991). "Diffusion in cementitious materials: 1. Comparative study of chloride and oxygen diffusion in hydrated cement pastes." *Cement and Concrete Research*, 21(4), 581-588.